



September 7. - 9.9.2009

Cheb, Czech Republic

STATIC CHARACTERISTICS OF COMPONENTS OF CONTROLLABLE THERMOELASTIC ACTUATOR

PROF. ING. IVO DOLEŽEL, CSc.
ING. VÁCLAV KOTLAN, Ph.D.
DOC. ING. BOHUŠ ULRYCH, CSc.

Abstract: *The paper deals with one of the basic conditions of practical employment of finely controllable thermoelastic actuators – problems of the static characteristics of its individual structural parts. It contains the formulation of the principle of such thermoelastic actuators, description of its components (a dilatation element heated by induction, auxiliary electromagnetic actuators, and self-locking friction clutches) and their mathematical models. Briefly discussed are also their corresponding computer models making use of the finite element method. The crucial point of the work consists in the presentation of the results – static characteristics of the considered structural parts of the controlled thermoelastic actuators.*

Key words: *Electromagnetic field, temperature field, field of, thermoelastic displacements, electromagnetic actuator, self-locking friction clutch, controllable dilatation, finite element method.*

INTRODUCTION

The paper deals with specific devices for realization of extremely small (on the order of $10^{-6} - 10^{-3}$ m) controllable shifts. Such devices can be used in a number of technical domains such as

- *optics* – for example, setting of focal distances of lens systems,
- *laser technologies* – setting of position or focusing of the laser beam,
- *microscope technologies* – setting of the position of specimens with respect to the focus of light beams in case of optical microscopes or focus of a beam of electrons in case of electron microscopes, and
- *acceleration of charged particles* – setting of the position of a target with respect to a beam of accelerated particles.

For realization of devices generating extremely small, controlled shifts, we can use the phenomenon of the thermal dilatation. Such a device works on the principle of common uncontrolled thermoelastic actuators (see [1], [2]). This device is, moreover, supplemented with some auxiliary parts (friction clutch, miniature electromagnetic actuator and some others) allowing its accurate control.

A detailed description of such controllable thermoelastic actuators and qualitative evaluation of their practical technological employment is discussed in [3]. The

presented paper deals with the quantitative static characteristics of the individual structural parts of these actuators that provide information necessary for their practical applications.

1 THE PROBLEM FORMULATION

The device represents a classical thermoelastic actuator [1], [2] that is supplemented by two miniature electromagnetic actuators supplied by pulse currents and two self-locking friction clutches controlled by these actuators. Its scheme is obvious from Fig. 1.

The harmonic current-carrying field coil **1** produces periodically varying magnetic field that generates eddy currents in the dilatation element **2** clamped in stiff wall (or flange) **4**. The hollow dilatation element contains thermal insulation **9** and working nonferromagnetic plunger **3** placed in two sliding bearings **7** and **8**. This plunger is controlled (fixed or released) by two conical self-locking friction clutches S_1 (**5**) and S_2 (**6**). These clutches are controlled by simple electromagnetic actuators A_1 consisting of steel cylinders and coils c_{11} , c_{12} and A_2 containing analogous coils c_{21} , c_{22} . Operation of these auxiliary actuators A_1 , A_2 and clutches S_1 , S_2 is controlled by pulse currents introduced into the mentioned coils $c_{11} - c_{22}$. These pulse currents can be rela-

tively strong (but short) in order that the forces generated by these actuators and self-locking friction forces are sufficiently high, but without any danger of overheating the coils.

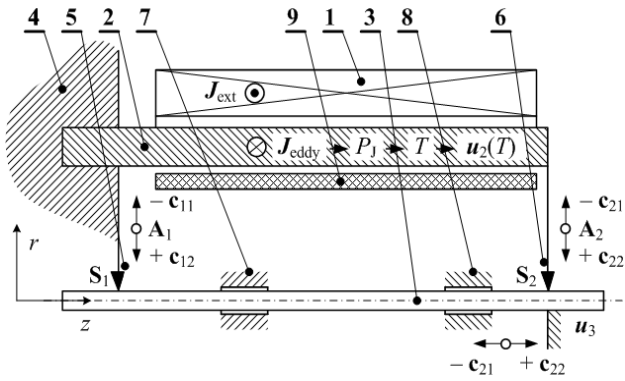


Fig. 1. Schematic arrangement of the controllable thermoelastic actuator:

1 – field coil, 2 – dilatation element, 3 – nonferromagnetic plunger, 4 – stiff fixing wall (flange), 5 – self-locking friction clutch S_1 controlled by actuator A_1 , 6 – other clutch S_2 controlled by actuator A_2 , 7, 8 – sliding bearings, 9 – thermal insulation

The detailed structural arrangement of the thermoelastic actuator with controllable working regime is shown in Fig. 2. The structures of the auxiliary electromagnetic actuators A_1 and A_2 is obvious from Figs. 3a and 3b and structures of self-locking friction clutches S_1 and S_2 in Figs. 4a and 4b.

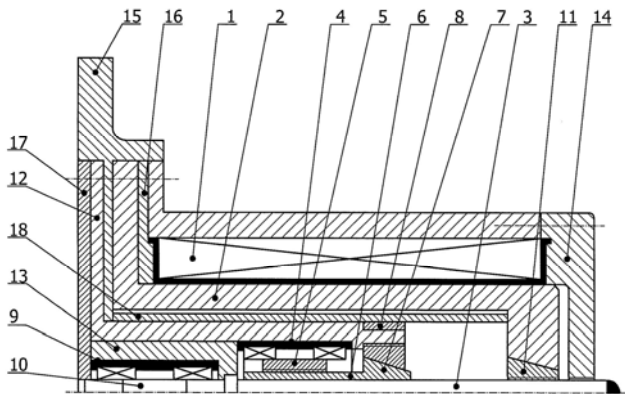


Fig. 2: Structural solution of the considered thermoelastic actuator:

1 – field coil with its shell, 2 – dilatation element, 3 – nonmagnetic plunger, 4, 5 – electromagnetic actuator A_1 of friction clutch S_1 , 6, 7 – friction clutch S_1 , 8 – fixing sleeve, 9, 10 – electromagnetic actuator A_2 of friction clutch S_2 , 11 – friction clutch S_2 , 12 – case of actuator A_1 , 13 – case of actuator A_2 , 14 – external shell of the thermoelastic actuator, 15 – fixing flange, 16 – internal strap, 17 – external strap, 18 – thermoinsulation case

The physical parameters of the individual structural parts of the thermoelastic actuator, as well as auxiliary electromagnetic actuators A_1 and A_2 and friction clutches S_1 and S_2 are listed in Tabs. 1–3.

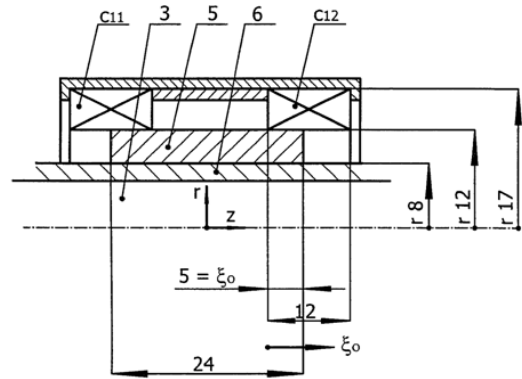


Fig. 3a: Arrangement of electromagnetic actuator A_1 :

5 – ferromagnetic hollow core (connected with 6), 6 – nonferromagnetic body of friction clutch S_1 , c_{11} and c_{12} – field coils of the actuator

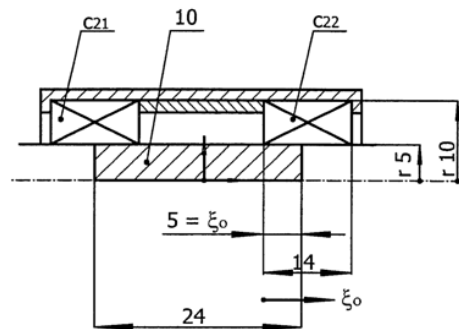


Fig. 3b: Arrangement of electromagnetic actuator A_2 :

10 – ferromagnetic core (connected with 3), c_{21} and c_{22} – field coils of the actuator

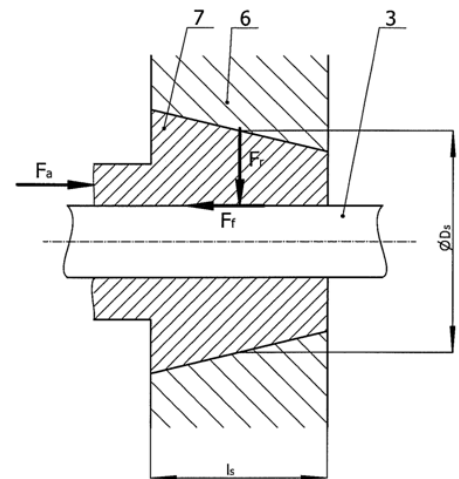


Fig. 4a: Friction clutch S_1 : 3 – nonferromagnetic plunger of the thermoelastic actuator, 6 – conical sleeve of clutch S_1 , 7 – conical body of clutch S_1

We can distinguish three working regimes of the device, but they can easily be combined to obtain much more sophisticated operation processes:

- The clutch S_2 is on, S_1 is off: if the element 2 dilates, the plunger 3 shifts with it. If element 2 is in rest, so is the plunger.
- The clutch S_1 is on, S_2 is off: the plunger 3 is in the stable position even when the element 2 dilates or

shifts back in the process of cooling.

- Both clutches S_1 and S_2 are off and current pulses are transferred to both auxiliary coils c_{21} and c_{22} . Thereby the plunger 3 is released and shifted to the starting position. Here it can be fixed by switching on the clutch S_1 .

Tab. 1: Physical parameters of the basic elements of the thermoelastic actuator (see Fig. 2)

	element	material	parameter	value	dim.		
1	field coil	Cu conductor	diameter of conductor D_c	1	mm		
			length of coil Δz	150	mm		
			thickness of coil Δr	16	mm		
			number of turns N_t	1250	—		
			filling coefficient κ	0.785	—		
			permeability μ_r	1	—		
			thermal conductivity (*) λ_T	306.1	W/m °C		
			electrical conductivity (*) γ_{el}	4.474×10^7	S/m		
2	dilat. element	carbon steel ČSN 12 040 [4]	characteristic $B(H)$	Fig. 5	—		
			thermal conductivity (*) λ_T	Fig. 6	—		
			electrical conductivity (*) γ_{el}	4.5×10^6	S/m		
			Young modulus E	2.1×10^{11}	N/m ²		
			Poisson number ν	0.3	—		
			coef. of thermal dilatation α_T	1.25×10^{-5}	1/°C		
3	plunger	Al	electrical conductivity (*) γ_{el}	3.5×10^7	S/m		
			permeability μ_r	1	—		
12 15	elements of the actuator (Fig. 2)	kevlar (TVA-RON)	thermal conductivity (*) λ_T	0.04	W/m °C		
			Young modulus E	1.24×10^{11}	N/m ²		
			Poisson number ν	0.3	—		
			coef. of thermal dilatation α_T	2×10^{-6}	1/°C		
			permeability μ_r	1	—		
18	thermally insulating shell (Fig. 2)	asbestos [6]	thermal conductivity (*) λ_T	0.1–0.3	W/m °C		
			permeability μ_r	1	—		
4 9	elements of the actuator (Fig. 2)	teflon [7]	permeability μ_r	1	—		
			thermal conductivity (*) λ_T	1.6	W/m °C		
13 14 16 17							

(*) modified with respect to the coefficient of filling

(**) unmovable air in the air gap, influence of convection neglected

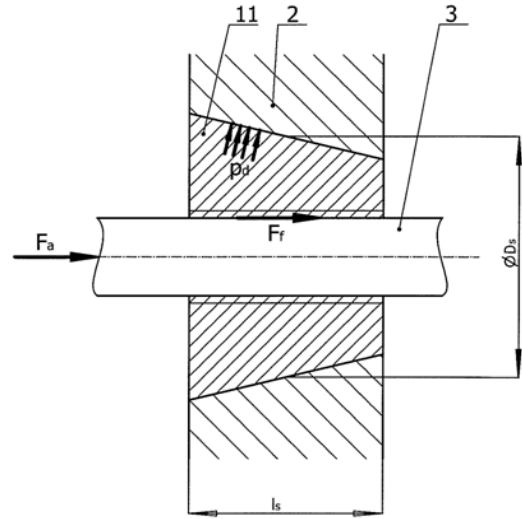


Fig. 4b: Friction clutch S_2 : 2 – dilatation element of the thermoelastic actuator, 3 – plunger of the thermoelastic actuator, 11 – conical body of clutch S_2

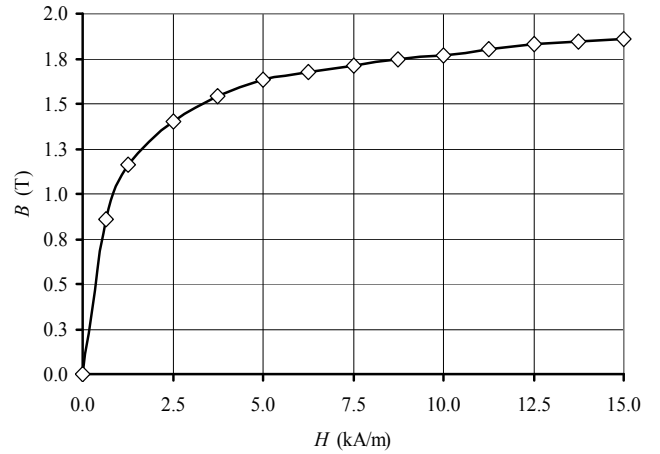


Fig. 5: Dependence $B(H)$ of steel CSN 12 040 (see [4])

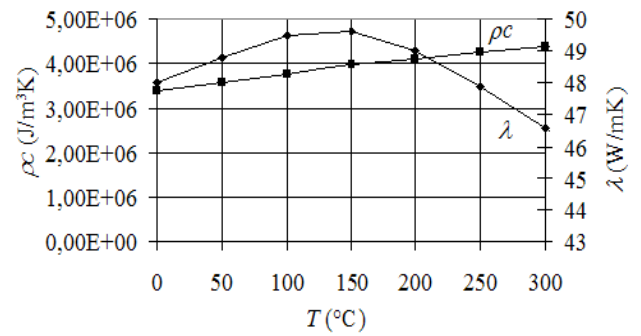


Fig. 6: Dependencies $\lambda = \lambda(T)$ and $\rho c = \rho c(T)$ for carbon steel 12 040

After formulating the mathematical model of the thermoelastic actuator (see [3]) that consists of three partial differential equations (PDEs) describing the electromagnetic field, temperature field and field of thermoelastic displacements and other structural parts (auxiliary actuators and self-locking friction clutches) it is possible to realize the discretized model whose numerical solution provides the operation characteristics of all basic components of the device.

Tab. 2: Physical parameters of the basic elements of the auxiliary actuators \mathbf{A}_1 and \mathbf{A}_2 (see Figs. 3a, 3b)

	element	material	parameter	value	dim.
$\mathbf{c}_{11}, \mathbf{c}_{12}$	field coils actuator \mathbf{A}_1	Cu conduc- tor	diameter of conductor D_c	1	mm
			length of coil Δz	12	mm
			thickness of coil Δr	5	mm
			number of turns N_t	60	–
			filling coefficient κ	0.785	–
			permeability μ_r	1	–
$\mathbf{c}_{21}, \mathbf{c}_{22}$	field coils actuator \mathbf{A}_2	Cu conduc- tor	diameter of conductor D_c	1	mm
			length of coil Δz	14	mm
			thickness of coil Δr	5	mm
			number of turns N_t	60	–
			filling coefficient κ	0.785	–
			permeability μ_r	1	–
3	plunger	Al	electrical conductivity γ_{el} permeability μ_r	3.5×10^7 1	S/m –
5 10	ferromagn. hollow core	carbon steel ČSN 12 040 [4]	characteristic $B(H)$ thermal conductivity λ_T	Fig. 5 Fig. 6	N/ m ² – 1/ °C
	ferromagn. full core		Young modulus E Poisson number ν coef. of thermal dilatation α_T	2.1×10^{11} 0.3 1.25×10^{-5}	
6	nonferro- magnetic body of the friction clutch	Al	see 3 , Fig. 4b		

2 OPERATION CHARACTERISTICS OF SELECTED ELEMENTS OF THE DEVICE

The thermoelastic actuator

For an illustration, we present static characteristics of the most important elements of the device in Fig. 2. Fig. 7 shows the distribution of the specific Joule losses p_j in the dilatation element **2** in the dependence on the field current density J_{ext} in the field coil **1** when its frequency $f = 50$ Hz. This dependence is slightly nonlinear, but it allows full controlling of these losses representing the sources of heat for the consequent nonstationary temperature field in interval $(5-25) \times 10^6$ W/m³, while the field current density changes in interval $(1-2) \times 10^7$ A/m².

Fig. 8 shows the evolution of the average temperature

T_a of the dilatation element **2** in time t , as a function of the field current density J_{ext} for frequency $f = 50$ Hz. It is obvious that the temperature T_a may also easily be controlled (in interval $90-280$ °C) when the field current density changes in interval $(1-2) \times 10^7$ A/m², within about 60 s. On the other hand, the value of T_a may easily exceed the temperature acceptable from the viewpoint of insulation of the field coil **1** (in our case 200 °C).

Tab. 3: Physical parameters of the basic elements of the friction clutches \mathbf{S}_1 and \mathbf{S}_2 (see Figs. 4a, 4b)

	element	material	parameter	value	dim.	
2	dilat. element	carbon steel ČSN 12 040 [4]	characteristic $B(H)$ thermal conductivity λ_T	Fig. 5		
			electrical conductivity γ_{el}	Fig. 6 4.5×10^6		S/m
			Young modulus E Poisson number ν	2.1×10^{11} 0.3		N/m ² –
			coef. of thermal dilatation α_T	1.25×10^{-5}		1/°C
3	plunger	Al	electrical conductivity γ_{el} permeability μ_r	3.5×10^7 1	S/m –	
6	conical sleeve of friction clutch \mathbf{S}_1	carbon steel ČSN 12 040 [4]	see 7 , Fig. 4a			
7	conical body of friction clutch \mathbf{S}_1	Al	see 3 , Fig. 4a			
11	conical body of friction clutch \mathbf{S}_2	Al	see 11 , Fig. 4b			

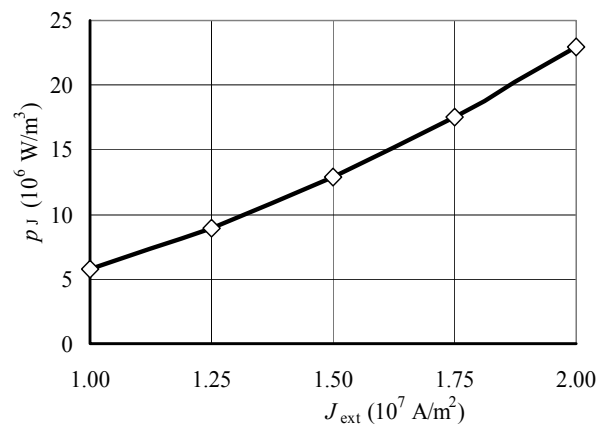


Fig. 7: Dependence of specific Joule losses p_j in dilatation element **2** on the field current density J_{ext} in field coil **1** ($f = 50$ Hz)

Figure 9 depicts the distribution of the maximum thermoelastic displacement $u_{z,max}$ of the dilatation element **2** in time t as a function of field current density J_{ext} in coil

1 (for frequency $f = 50$ Hz). It is clear that the corresponding shifts may be regulated in a relatively wide interval $(15-60) \times 10^{-5}$ m by current $J_{\text{ext}} \in \langle 1-2 \rangle \times 10^7$ A/m² within about 60 s. But even here some of the dilations may be physically unreal due to unacceptable temperatures (see the discussion to Fig. 8).

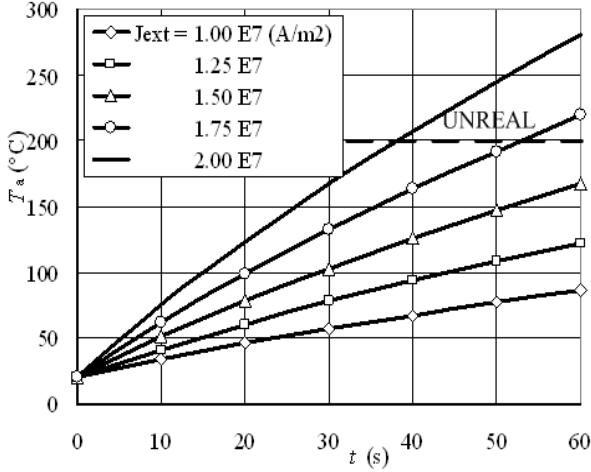


Fig. 8: Distribution of the average temperature T_a of the dilatation element 2 in time t as a function of field current density J_{ext} (for $f = 50$ Hz)

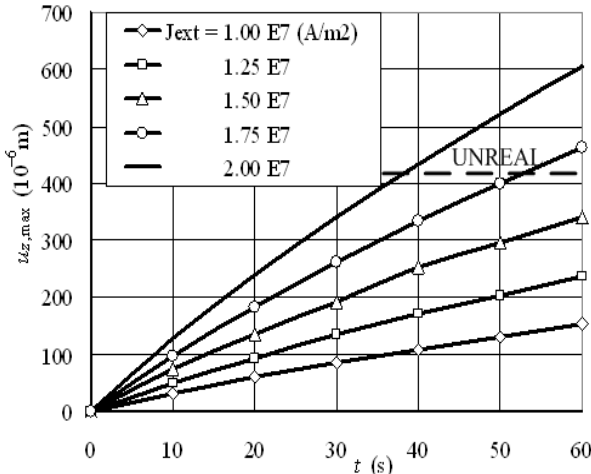


Fig. 9: Distribution of maximum thermoelastic displacement $u_{z,\text{max}}$ of the dilatation element 2 in time t as a function of field current density J_{ext} (for $f = 50$ Hz)

Fig. 10 contains the time evolution of maximum values of reduced stress $\sigma_{\text{red,max}}$ of the dilatation element 2 according to the van Mises hypothesis (see, for example, [8]) as a function of J_{ext} in the field coil 1 for frequency $f = 50$ Hz. For steel CSN 12 040 used for the dilatation element the yield stress $\sigma_K = 300$ MPa (see, for example, [9]), and this value is not exceeded in our case. But similarly as in previous cases, unacceptable can become the temperature (see discussions to Figs. 8 and 9).

The auxiliary actuators A_1 and A_2

The operation characteristics of auxiliary actuators A_1 and A_2 (Figs. 3a and 3b) are presented in Figs. 11,

12, and 13. Fig. 11 depicts the static characteristic of actuator A_1 and Fig. 12 an analogous characteristic for A_2 . It is clear that the forces $F_{m,z}$ generated by the actuators:

- Strongly depend on the field current density J_{ext} (for $J_{\text{ext}} \in \langle 1-2 \rangle \times 10^7$ A/m² these forces lie in interval $\langle 0, 400 \rangle$ N),
- Depend also on the position of the ferromagnetic hollow core 5 of the actuators with respect to their field coils $c_{11} \dots c_{22}$ (coordinate ζ , see Figs. 3a and 3b). This dependence exhibits an extreme, i.e., there exist an optimum position ζ_{opt} for which the force $F_{m,z}$ reaches its maximum (at a given J_{ext}).

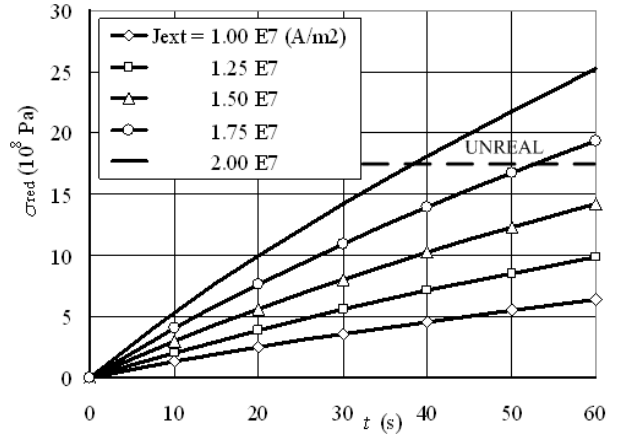


Fig. 10: Distribution of the reduced stress σ_{red} (according to the van Mises hypothesis) of the dilatation element 2 in time t as a function of field current density J_{ext} (for $f = 50$ Hz)

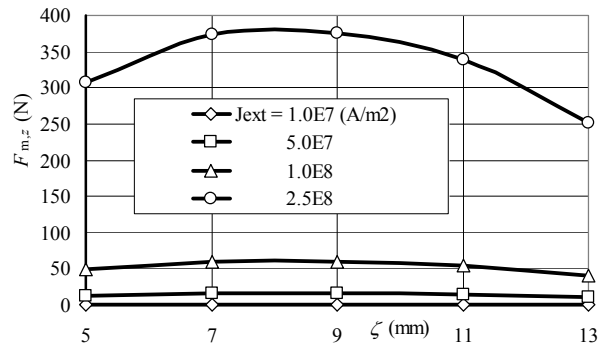


Fig. 11: Static characteristic of actuator A_1

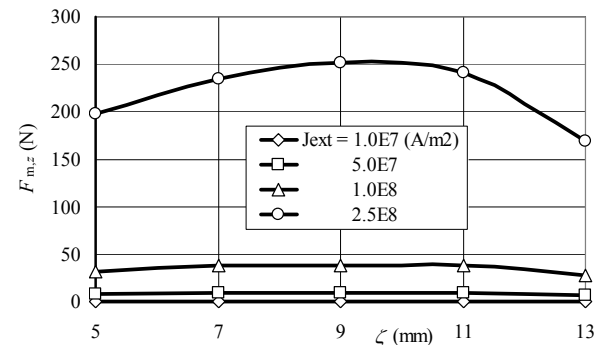


Fig. 12: Static characteristic of actuator A_2

Figure 13 depict the maximum forces $F_{m,z,max}$ that may be generated by both actuators \mathbf{A}_1 and \mathbf{A}_2 at a given value of the field current density J_{ext} .

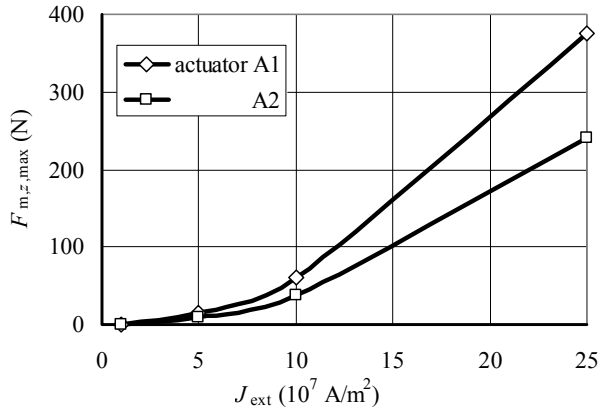


Fig. 13: Maximum forces $F_{m,z,max}$ of actuators \mathbf{A}_1 and \mathbf{A}_2 as functions of field current density J_{ext}

The self-locking friction clutches \mathbf{S}_1 and \mathbf{S}_2

The operation characteristics of clutches \mathbf{S}_1 and \mathbf{S}_2 are shown in Figs. 14, 15, and 16. Figures 14 and 15 show the dependencies of the pressure p_d over the conical surfaces of the clutches on the axial force $F_a \approx F_{m,z}$ generated by actuators \mathbf{A}_1 and \mathbf{A}_2 . As the maximum acceptable pressure for both clutches $p_{d,max} \in \langle 0.3-5.0 \rangle$ MPa [11], it is clear that both of them can transfer even much higher forces than we consider. From the viewpoint of suitability, it is better to use clutches of greater lengths l_s and greater angle of conicity α .

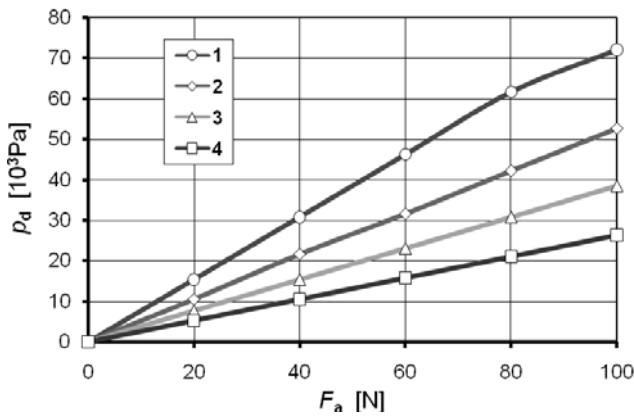


Fig. 14: Dependence of pressure p_d in the conical surface of clutch \mathbf{S}_1 on force F_a generated by actuator \mathbf{A}_1
1 – $l_s = 20$ mm, $\alpha = 15^\circ$, **2** – $l_s = 20$ mm, $\alpha = 30^\circ$,
3 – $l_s = 40$ mm, $\alpha = 15^\circ$, **4** – $l_s = 40$ mm, $\alpha = 30^\circ$

Finally, Fig. 16 shows the dependence of the friction force F_f between the plunger **3** and internal cylindrical surface of the conical body **7** of the friction clutch \mathbf{S}_1 on the axial force F_a generated by actuators \mathbf{A}_1 and \mathbf{A}_2 . It is obvious that from the viewpoint of this force smaller angles α are better.

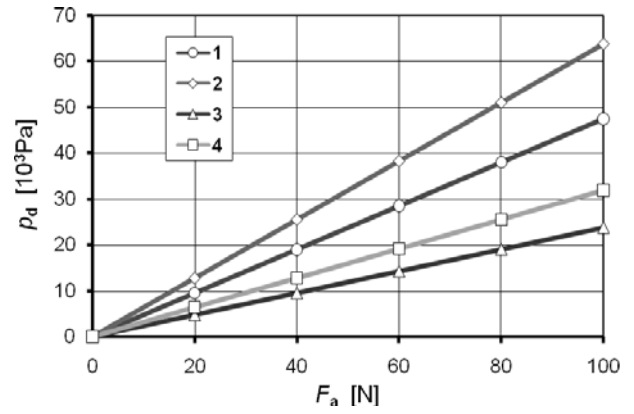


Fig. 15: Dependence of pressure p_d in the conical surface of clutch \mathbf{S}_2 on force F_a generated by actuator \mathbf{A}_2
1 – $l_s = 20$ mm, $\alpha = 15^\circ$, **2** – $l_s = 20$ mm, $\alpha = 30^\circ$,
3 – $l_s = 40$ mm, $\alpha = 15^\circ$, **4** – $l_s = 40$ mm, $\alpha = 30^\circ$

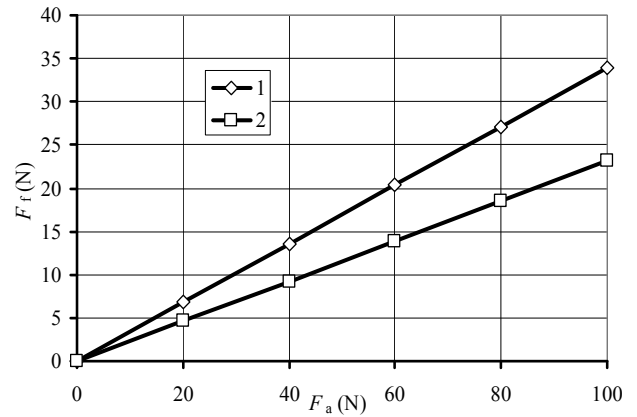


Fig. 16: Dependence of the friction force F_f in clutch \mathbf{S}_1 on the axial force F_a generated by actuator \mathbf{A}_1
line **1** – $\alpha = 15^\circ$, line **2** – $\alpha = 30^\circ$

3 CONCLUSION

A more detailed description of the considered controllable actuator and its characteristics may be found in [3]. But its complete description and its technological employment is presented on www pages <http://147.228.94.30/> of the Czech electronical journal Electroscop.

REFERENCES

- [1] Doležel, I., Karban, P., Ulrych, B., Pantelyat, M., Matyukin, Y., Gontarowskiy, P.: Numerical Model of a Thermoelastic Actuator Solved as a Coupled Contact Problem. COMPEL, Vol. 26, 2007, No. 4, pp.1063–1072.
- [2] Pantelyat, M., Matyukin, Y., Gontarowskiy, P., Doležel, I., Ulrych, B.: Computer Simulation of Actuators Working on Principle of Thermoelasticity. Proc. ICEM 2006, 2–5. 09. 06. Chania, Greece. Book of Abstracts, pp. 272.
- [3] Doležel, I., Krónerová, E., Ulrych, B.: Induction Thermoelastic Actuator with Controllable Operation Regime. ISEF 2009 - XIV International Symposium

on Electromagnetic Fields, Arras, France, September 2009, accepted.

- [4] Company standard SKODA 00 6004 (in Czech).
- [5] www.azom.com (June 2009)
- [6] Mikulčák, J. et al: Mathematical, Physical and Chemical Tables (in Czech). SPN Praha, 1970.
- [7] Hassdenteufel, J., Květ, K. et al: Materials for Electrical Engineering (in Czech). SNTL Praha, 1967.
- [8] Černoch, S.: Tables for Technical and Mechanical Engineering (in Czech). SNTL Praha, 1977.
- [9] <http://www.vitkovicesteel.com/produkty-detail/produkty/-1/produkty-podsekce/plechy-z-konstrukcnich-oceli-2/produkty-detail/plechy-z-oceli-podle-en-10025-2-2/> (July 2009).
- [10] Hosnedl, S., Krátký, J.: Booklet of Mechanical Engineer 1, General machine parts (in Czech). Computer Press, Brno, 1999.
- [11] www.diafrikt.cz.

Authors: Prof. Ing. Ivo Dolezel, CSc., Czech Technical University, Faculty of Electrical Engineering, Technická 2, 166 27 Prague, CR, E-mail: dolezel@fel.cvut.cz; Ing. Vaclav Kotlan, PhD., Assoc. Prof. Ing. Bohus Ulrych, CSc., University of West Bohemia, Faculty of Electrical Engineering, Univerzitní 26, 306 14 Pilsen, CR, E-mail: {vkotlan, ulrych}@kte.zcu.cz